

# Long-memory effects in linear-response models of Earth's temperature and implications for future global warming

MARTIN RYPDAL\* AND KRISTOFFER RYPDAL

*Department of Mathematics and Statistics, University of Tromsø, Norway.*

## ABSTRACT

A linearized energy-balance model for global temperature is formulated, featuring a scale-free long-range memory (LRM) response and stochastic forcing representing the influence on the ocean heat reservoir from atmospheric weather systems. The model is parametrized by an effective response strength, the stochastic forcing strength, and the memory exponent. The instrumental global surface temperature record and the deterministic component of the forcing are used to estimate these parameters by means of the maximum-likelihood method. The residual obtained by subtracting the deterministic solution from the observed record is analyzed as a noise process and shown to be consistent with a long-memory time-series model and inconsistent with a short-memory model. By decomposing the forcing record in contributions from solar, volcanic, and anthropogenic activity one can estimate the contribution of each to 20'th century global warming. The LRM model is applied with a reconstruction of the forcing for the last millennium to predict the large-scale features of northern hemisphere temperature reconstructions, and the analysis of the residual also clearly favors the LRM model on millennium time scale. The decomposition of the forcing shows that volcanic aerosols give a considerably greater contribution to the cooling during the Little Ice Age than the reduction in solar irradiance associated with the Maunder minimum in solar activity. The LRM model implies a transient climate response in agreement with IPCC AR4 projections, but the stronger response on longer time scales suggests to replace the notion of equilibrium climate sensitivity by a time-scale dependent sensitivity.

## 1. Introduction

When the climate system is subject to radiative forcing the planet is brought out of radiative balance and the thermal inertia of the planet makes the surface temperature lag behind the forcing. The time constant  $\tau$ , which is the time for relaxation to a new equilibrium after a sudden change in forcing, has been considered to be an important parameter to determine. The equilibrium climate sensitivity  $S_{\text{eq}}$ , the temperature raise per unit forcing after relaxation is complete, is another. In the industrialized epoch a major source for the present energy imbalance is the steady increase in anthropogenic forcing. If the climate system can be modeled as a hierarchy of interacting subsystems with increasing heat capacities and response times there will also be a hierarchy of climate sensitivities. One way of modeling this feature is to replace the standard exponentially decaying impulse-response function  $G(t) \sim e^{-t/\tau}$  with one that is scale free, i.e., decaying like a power law;  $G(t) \sim t^{\beta/2-1}$ . For a climate system which is subject only to random forcing modeled as a white Gaussian noise, and if  $0 < \beta < 1$ , the resulting climate variable  $T(t)$  is then a long-memory fractional Gaussian noise (fGn) with a power spectral density (PSD) of the form  $\mathcal{P}(f) \sim f^{-\beta}$  (Beran

1994; Embrechts and Maejima 2002). The response to a step at time  $t = 0$  in the forcing is then  $\int_0^t G(t) dt \sim t^{\beta/2}$ . Hence,  $S_{\text{eq}}$  is infinite for such a perfectly scale-free response function, since the response to an increase in the forcing will never saturate. This is of course unphysical, but rather than invalidating the scale-free response model it suggests the introduction of a frequency-dependent climate sensitivity  $S(f)$ . Even in the exponential response model the amplitude response to an oscillation vanishes for high frequencies, but converges to  $S_{\text{eq}}$  as  $f \rightarrow 0$ . In the scale-free response model  $S(f)$  diverges in the low-frequency limit, and hence there is of course a cut-off frequency  $f_c = 1/t_c$  corresponding to a time-scale  $t_c$  after which the scale-free response is no longer valid. In this paper, however, we present evidence for power-law scaling with  $\beta \approx 1$  in the global temperature response over time scales of many centuries (Rybski et al. 2006; Rypdal et al. 2013), suggesting that a lower bound for  $t_c$  exceeds century time scales. We shall demonstrate that long-memory responses can explain important aspects of Northern hemisphere temperature variability over the last millennium and lead to new predictions of how much more warming there will be “in the pipeline” in any given forcing scenario (Hansen et al.

2005, 2011).

Previous work on long-range memory (LRM) in climate records all hypothesize that the signal is composed of an LRM noise superposed on a trend driven by external forcing, and hence the methods are designed to eliminate such trends. The degree of detrending, however, is a parameter subject to choice. Choosing it too low implies that the detrending is incomplete, leading to overestimation of the memory exponent. Choosing it too high implies elimination of some of the internal noise and underestimation of the memory. Another source of error is that the concept of a slow trend does not always reflect the true nature of deterministic forced variability. Some components of the forcing may be faster than important components of the internal variability, and hence precise separation of internal from forced variability can only be done by using information about the deterministic component of the forcing record. Fortunately, such reconstructions of the forcing records exist and are used as input for historic runs of climate models.

We contend that correct estimation of the LRM-properties of the internal climate variability can only be done by analyzing the residue obtained by subtracting the forced deterministic component of the climate signal. We shall show that the climate response function is all we need to predict both the deterministic component of the climate signal and the memory properties of the internal variability.

## 2. Linear response models

Linear response models of Earth's surface temperature have been considered by several authors, see e.g. Hansen et al. (2011) and Rypdal (2012). The physical backbone is the zero-dimensional, linearized energy-balance equation derived for instance in the appendix of (Rypdal 2012). It has the form

$$\frac{dQ}{dt} + \frac{1}{S_{\text{eq}}}T = F, \quad (1)$$

where  $Q$  is the total energy content of the climate system.  $F$  and  $T$  are perturbations of radiative influx and surface temperature relative to a reference state in radiative equilibrium, i.e., a state where the radiative influx absorbed by the Earth surface balances the infrared radiation emitted to space from the top of the troposphere. For a given influx the equilibrium outflux is controlled by the Stefan-Boltzmann radiation law and complex feedback processes which determine the equilibrium climate sensitivity  $S_{\text{eq}}$  (see e.g., Eqs. (A5-A7) in Rypdal (2012)). The true value of  $S_{\text{eq}}$  is subject to considerable controversy due to insufficient knowledge of some of these feedbacks, and because they operate on wildly different time scales.

The exponential response model is obtained by introducing an effective heat capacity  $C$  of the climate system such that  $dQ = CdT$ , and introducing the time constant

$\tau = CS_{\text{eq}}$ . Eq. (1) then takes the form

$$\mathcal{L}T = F, \quad (2)$$

where the linear operator  $\mathcal{L} \equiv C^{-1}(d_t + \tau^{-1})$  has the Green's function  $G(t) = C^{-1} \exp(-t/\tau)$ . The scale-free response model corresponds to replacing  $\mathcal{L}$  by a fractional derivative operator (see Rypdal (2012) for details) which effectively corresponds to replacing the exponential Green's function with the power-law function  $G(t) = (t/\mu)^{\beta/2-1}\xi$ , where  $\mu$  is a scaling factor in the units of time characterizing the strength of the response and  $\xi \equiv 1 \text{ Km}^2/\text{J}$  is a factor needed to give  $G(t)$  the right physical dimension.

We shall define our equilibrium reference state such that  $T$  is the temperature relative to the initial temperature  $\hat{T}_0$  in the observed record, i.e.,  $T = \hat{T} - \hat{T}_0$ , where the  $\hat{\phantom{x}}$  symbol means that temperature is measured relative to absolute zero (Kelvin). The observed record then has  $T(0) = 0$ . This means that we define  $F$  as the influx relative to the influx which balances the outflux at this initial temperature, and since the system is not necessarily in equilibrium at  $t = 0$ , we generally have that  $F(0) \neq 0$ . Since  $F(0)$  is not known a priori it becomes a parameter to be estimated along with other model parameters. According to these conventions the temperature evolution according to linear response theory becomes

$$\hat{T} = \hat{T}_0 + F(0) \int_0^t G(t-s) ds + \int_0^t G(t-s) \tilde{F}(s) ds, \quad (3)$$

where we have introduced  $\tilde{F}(t) \equiv F(t) - F(0)$ . In principle, we could have chosen  $F(0) = 0$  and  $T(0) \neq 0$ , but then we would for the scale-free response have to face an initial value problem for a fractional differential equation, which is not well posed. For the exponential response model Eq. (3) takes the form

$$\hat{T} = \hat{T}_0 + S_{\text{eq}}F(0)(1 - e^{-t/\tau}) + \frac{1}{C} \int_0^t e^{-(t-s)/\tau} \tilde{F}(s) ds. \quad (4)$$

Suppose the evolution of the forcing prior to the time  $t = 0$  has given rise to an energy imbalance expressed through a non-zero  $F(0)$ , and that the forcing remains constant at this level ( $\tilde{F}(t) = 0$ ) in the subsequent evolution. Then equation (4) shows an exponential relaxation to a new equilibrium state with temperature  $\hat{T} = \hat{T}_0 + S_{\text{eq}}F(0)$ . For the scale-free response model the corresponding expression takes the form

$$\hat{T} = \hat{T}_0 + \frac{2\xi\mu F(0)}{\beta} \left(\frac{t}{\mu}\right)^{\beta/2}. \quad (5)$$

The unlimited growth of the temperature in response to the initial step in forcing appears to be unphysical. For instance, Eq. (1) implies that  $dQ/dt$  goes negative for  $t > t_c$ , where

$$t_c \sim \mu \left(\frac{S_{\text{eq}}\beta}{2\xi\mu}\right)^{2/\beta}. \quad (6)$$

One solution to this paradox could be that the power-law tail in the response exhibits an exponential cut-off for  $t > t_c$ . We shall see, however, that for generally accepted values of  $S_{\text{eq}}$  the cut-off time is not more than a hundred years, while we find evidence for power-law scaling up to a millennium at least. Another solution to the paradox could be that Eq. (1) is too simplistic. The equilibrium climate sensitivity is traditionally defined from the end state of long model integrations subject to various forcing scenarios. It is difficult to decide if the models have attained equilibrium at the end of the integration, and  $S_{\text{eq}}$  will depend critically on conventions that distinguish between forcing and feedbacks. It is also conceivable that  $S_{\text{eq}}$  is path-dependent, i.e., dependent on the forcing history. This issue is discussed further in section 6, after we have established the full implications of the LRM response model.

### 3. Dynamic-stochastic models

In Rypdal (2012) it was shown that the scale-free response function gives a somewhat better characterization of the observed record, but no systematic method was presented which would allow rejection of the exponential response hypothesis in favor of the scale-free response hypothesis. The clue to develop such a method is to address the apparently random fluctuations in the observed record that makes it deviate from the solution to the response model under the prescribed forcing. The forcing given by Hansen et al. (2011) is a deterministic function and the corresponding response should therefore be perceived as a deterministic solution. Even with a correct model of the response the deterministic solution will not be a perfect match to the observed record because the forcing should also have a stochastic component corresponding to the random forcing of the ocean-land heat content from the atmospheric weather systems. A more complete (dynamic-stochastic) model can be constructed by adding a stochastic forcing such that Eq. (2) is generalized to

$$\mathcal{L} dT(t) = dF_d(t) + \sigma dB(t). \quad (7)$$

Here  $F_d(t)$  is the deterministic component of the forcing and  $B(t)$  is the Wiener process, sometimes called a Brownian motion. We have introduced an unknown parameter  $\sigma$  denoting the standard deviation of the stochastic forcing. There are two major advantages of introducing the stochastic forcing:

(i) Since the observed record in this formulation should be perceived as one realization of a stochastic process produced by the dynamic-stochastic model the residual difference between this record and the deterministic solution should be perceived as a noise process  $\tilde{T}(t)$  given by the

stochastic part of Eq. (7), i.e.,

$$\tilde{T}(t) = \sigma \int_0^t G(t-s)dB(s). \quad (8)$$

By using the exponential response model, Eq. (8) produces the Ornstein-Uhlenbeck stochastic process. On time scales less than  $\tau$  this process has the non-stationary character of a Brownian motion and the PSD has the power-law form  $\mathcal{P}(f) \sim f^{-2}$  for  $f > \tau^{-1}$ . On time scales greater than  $\tau$  the process has the stationary character of a white noise and the PSD is flat for  $f < \tau^{-1}$ . Actually, the PSD has the form of a Lorentzian,  $\mathcal{P}(f) \sim [\tau^{-2} + (2\pi f)^2]^{-1}$ . For a discrete-time process the direct analog to the Ornstein-Uhlenbeck process is the first-order autoregressive process AR(1). The scale-free response model, on the other hand, produces a fractional Gaussian noise (fGn) for  $-1 < \beta < 1$  and a fractional Brownian motion (fBm) for  $1 < \beta < 3$ . For these noises and motions the PSD for low frequencies has the power-law form  $\mathcal{P}(f) \sim f^{-\beta}$ . In principle, an estimator for the PSD (like the periodogram) applied to the observed residual could be compared to the PSD for the two response models to test the validity of the models against each other. In practice, other estimators in this paper will be used, but the idea is the same.

(ii) Formulating the problem as a parametric stochastic model allows systematic estimation of the parameters  $\{F(0), C, \sigma, \tau\}$  for the exponential model, and  $\{F(0), \mu, \sigma, \beta\}$  for the scale-free model. The method is based on maximum-likelihood estimation (MLE) which establishes the most likely parameter set that could produce the observed record from the prescribed forcing. The principles of the MLE employed here are explained in the appendix.

The significance of the LRM response can be appreciated by looking at equation (2) in the Fourier domain;

$$\tilde{T}(f) = \tilde{G}(f)\tilde{F}(f), \quad (9)$$

where  $\tilde{T}, \tilde{G}, \tilde{F}$  are Fourier transforms of  $T, G, F$ , and  $\tilde{G}(f)$  is the transfer function of the linear system. This relation naturally leads us to define the frequency-dependent sensitivity as

$$S(f) = |\tilde{G}(f)| = \frac{|\tilde{T}(f)|}{|\tilde{F}(f)|}. \quad (10)$$

For the exponential response model we find

$$S(f) = \frac{1}{C\sqrt{\tau^{-2} + (2\pi f)^2}}, \quad (11)$$

which in the limit  $2\pi f\tau \ll 1$  converges to the equilibrium sensitivity  $S_{\text{eq}} = \tau/C$ . For the LRM model we have

$$S(f) = \frac{\xi\mu\Gamma(\beta/2)}{|2\pi\mu f|^{\beta/2}}, \quad (12)$$

where  $\Gamma(x)$  is the Euler Gamma function. In Fig. 1 we show a plot of  $S(f)$  for the values of the model parameters estimated for the global temperature and forcing record in section 4. Note that the frequency-dependent sensitivities for the two models depart substantially from each other only for frequencies corresponding to time scales longer than a century. Hence it is on these slow time-scales that LRM really has serious impact on the climate dynamics. The dramatic consequences will be apparent when we consider time-scales of many centuries in section 5.

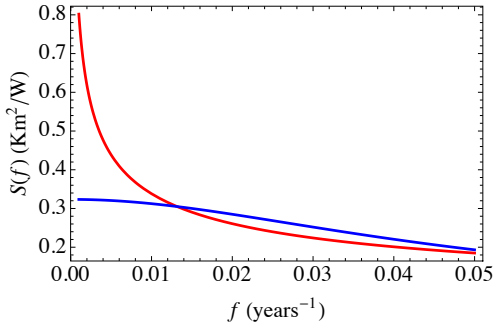


FIG. 1. Frequency-dependent sensitivity  $S(f)$  for the exponential response model (blue) and the scale-free model (red) for model parameters given in Tab. 1.

In principle, the right-hand-side of Eq. (10) could be used to estimate  $S(f)$  directly from Fourier transforming the temperature and forcing records, and then to compare with Eqs. (11) and (12) to assess the validity of the two response models. The short length of the records, however, make the Fourier spectra very noisy, and the ratio between them even more so. Additional complications are that the spiky nature of the forcing record to volcanic eruptions and the unknown amplitude of the stochastic forcing component. Hence, we have to resort to the model parameter estimation described above, and to other estimators than the Fourier transform, to settle this issue.

#### 4. Parameter estimation from instrumental records

The temperature data sets analyzed in this section can be downloaded from the Hadley Center Met Office web site. We consider the global mean surface temperature (GMST) as presented by the HadCRUT3 monthly mean or annual mean temperatures (Brohan et al. 2006). The forcing record is the one developed by Hansen et al. (2005) and used by Hansen et al. (2011) and, and is shown in Fig. 2a. The forcings decomposed into volcanic, solar, and anthropogenic contributions are shown in Figs. 2 b,c,d, respectively. The forcing records go from 1880 till 2010 with annual resolution, so even if the temperature record goes further back in time and has monthly resolution, the maximum-likelihood estimation of model parameters only employs the

130 yr records with annual resolution. The analysis of the residual noise signal, however, utilizes the monthly resolution to improve the statistics.

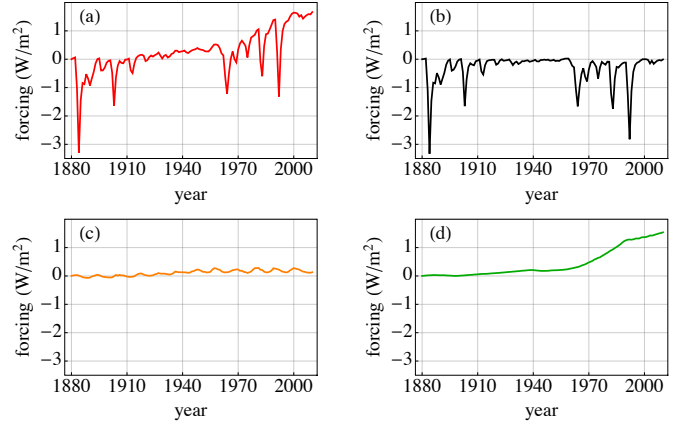


FIG. 2. (a) Total forcing 1880-2010 A.C. (b) Volcanic forcing. (c) Solar forcing. (d) Anthropogenic forcing.

Exponential response model	Scale-free response model
$\tau = 4.3 (\pm 0.7)$ years	$\beta = 0.75 (\pm 0.12)$
$C = 4.2 (\pm 0.2) \times 10^8$ J/m <sup>2</sup>	$\mu = 8.4 (\pm 2.5) \times 10^{-3}$ years
$F_0 = 0.19 (\pm 0.12)$ W/m <sup>2</sup>	$F_0 = 0.19 (\pm 0.16)$ W/m <sup>2</sup>
$\sigma_{\tilde{T}} = 0.15 (\pm 0.01)$ K	$\sigma_{\tilde{T}} = 0.13 (\pm 0.02)$ K

TABLE 1. The ML estimates of parameters in the exponential response model and in the scale-free response model. The parameters are estimated from the HadCRUT3 annual temperature record. The parameters  $\sigma_{\tilde{T}}$  are defined as the standard deviation of the stochastic components  $\tilde{T}(t)$ . The numbers in the brackets are the mean standard errors obtained from a Monte-Carlo study.

The results of the MLE method for the exponential and scale-free models are given in Tab. 1. The heat capacity  $C = 4.2 \times 10^8$  J/m<sup>2</sup> estimated from the exponential model is very close to that of a 100 m deep column of sea water, and the time constant 4.3 yr is in the middle of the range (3-5 yr) observed by Held et al. (2010) from instantaneous CO<sub>2</sub> experiments with the CM2.1 model. What was also observed in those model runs was an additional slower response which showed that equilibrium was not attained after 100 yr of integration, indicating that the exponential model does not contain the whole story. In Fig. 3a we present the deterministic part of the solutions for both models along with the observed GMST record. Although the the solution of the scale-free model seems to yield a somewhat better representation of both the multi-decadal variability and the response to volcanic eruptions, the difference between the deterministic solutions of the

two models is not striking on these time scales. The reason for this can be understood from Fig. 1. It is on time scales longer than a century that the difference will become apparent. For the stochastic part of the response, however, the two models can be tested against data on all observed time scales. Such a test is performed in Fig. 3b, where the residual noise (the observed GMST with the deterministic solution subtracted) has been analyzed by the wavelet-variance technique (Flandrin 1992; Rypdal et al. 2013). What is plotted here is the variance of the Mexican-hat wavelet coefficient of the residual noise versus wavelet scale. For an AR(1) process (stochastic solution of the exponential model) the slope of this curve in a log-log plot is near 2 for time scales much less than  $\tau$ , and near 0 for time scales much greater than  $\tau$ , as shown by the blue dashed curve in the figure. For an fGn the slope of the curve is  $\beta$ , which has been estimated to be  $\beta \approx 0.75$ , as shown by the red dashed curve. The wavelet variance of the actual observed residuals with reference to the two models are shown as the blue crosses and the red circles in the figure, and shows that the residuals are inconsistent with an AR(1) process, but consistent with an fGn process.

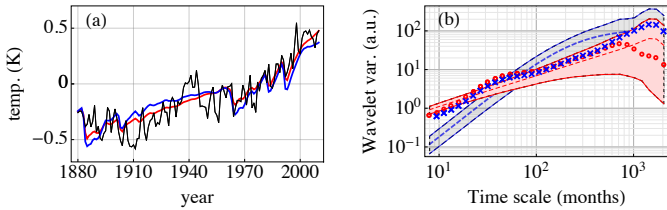


FIG. 3. (a) Deterministic part of the solution. Blue: for the exponential response model. Red: for the scale-free response model. Black: the HadCRUT3 annual temperature record. (b) Blue crosses: Wavelet variance of monthly GMST record with deterministic solution of exponential response model subtracted. Red circles: the same with deterministic solution of scale-free model subtracted. Blue dashed: Ensemble mean of wavelet variance of simulated AR(1) process with estimated parameters from the exponential response model. Shaded blue area marks  $2 \times$  standard deviation of the distribution of wavelet variances over the ensemble. Red dashed and shaded area: the same for an fGn process with estimated parameters from the scale-free model. The wavelet used is the Mexican-hat wavelet, and the time scale on the horizontal axis is the wavelet-scale multiplied by 4, which corresponds closely to the oscillation period in the periodogram.

In Fig. 4 we demonstrate that the observed record falls within the uncertainty range of the two dynamic-stochastic models. Here we have generated an ensemble of solutions to the two models with the estimated parameters and plot-

ted the  $2\sigma$  range around the deterministic solutions. The results are shown as the two shaded areas in Figs. 4a and 4b, respectively.

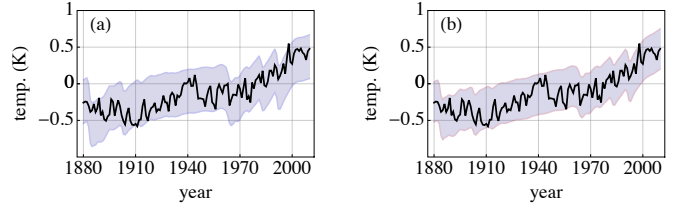


FIG. 4. Black curves are the GMST record. Shaded areas are the deterministic part of the solution  $\pm 2 \times$  standard deviation of the stochastic part representing the range of solutions to the model. (a) for the exponential response model. (b) for the scale-free response model.

In Fig. 5 we plot the deterministic scale-free response to the total forcing along with the separate responses to the volcanic, solar, and anthropogenic forcing components. During the first half of the 20<sup>th</sup> century solar and anthropogenic forcing contribute equally to the global warming trend. After 1950 there is a significant cooling trend due to volcanic aerosols, a weaker warming contribution from solar activity, and a dominating anthropogenic warming.

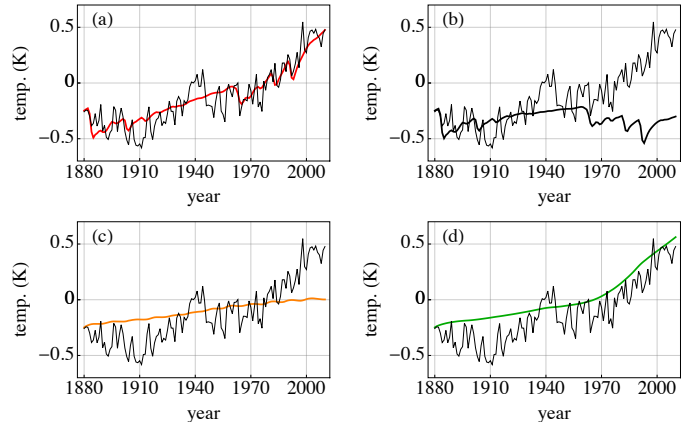


FIG. 5. Deterministic part of forced temperature change 1880-2010 A.C. according to the scale-free model. (a) From total forcing. (b) From volcanic forcing. (c) From solar forcing. (d) From anthropogenic forcing.

## 5. Predicting reconstructed records

The wavelet variance plotted in Fig. 3b can only demonstrate that the residual is scale free up to time scales less than the length of the 130 yr record. Verifying LRM on longer time scales requires longer records. This was done

by Rybski et al. (2006) and Rypdal (2012) using detrending techniques like the wavelet variance applied directly to reconstructed temperature records over the last one or two millennia. Here we shall utilize a forcing record for the last millennium (Crowley 2000) which is shown in Fig. 6, with its decomposition in volcanic, solar, and anthropogenic contributions. Many temperature reconstructions for the

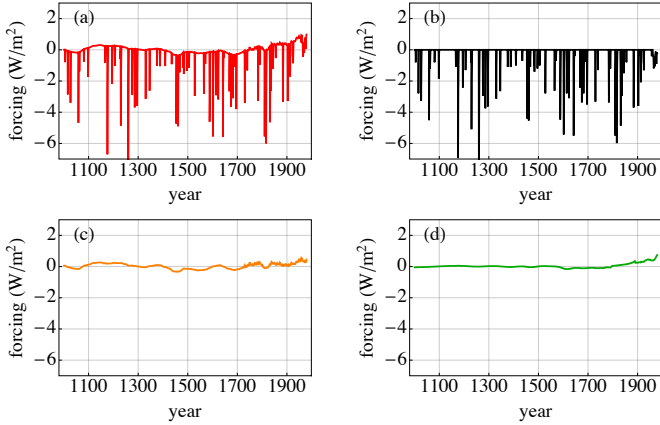


FIG. 6. (a) Total forcing 1000-1978 A.C. (b) Volcanic forcing. (c) Solar forcing. (d) Anthropogenic forcing.

Northern hemisphere exist for this time period (see Rybski et al. (2006) for a selection). We shall employ our dynamical-statistical models to the reconstruction by Moberg et al. (2005), which shows a marked temperature difference between the Medieval Warm Period (MWP) and the Little Ice Age (LIA). For the scale-free model the model parameters estimated from Crowley forcing and Moberg temperature are very close to those estimated from the instrumental records, except for the initial forcing  $F(0)$ . The initial forcing measures how far the climate system is from equilibrium at the beginning of the record, and this will depend on at what time this beginning is chosen. Considering that the timing of volcanic events and the corresponding temperature responses probably are subject to substantial errors in these reconstructions, this might give rise to errors in the parameter estimates. For this reason we have also estimated  $F(0)$  from Crowley forcing and Moberg temperature by retaining the values of the other parameters estimated from the instrumental record and shown in Tab. 1. The resulting deterministic solutions for the two models are plotted in Fig. 7a, along with the Moberg record. Since only the departure from equilibrium forcing  $F(0)$  are estimated from the reconstruction data, these solutions should be considered as “predictions” of the deterministic component of the forced evolution over the last millennium, based on parameters estimated from the modern instrumental records. The exponential model predicts too low temperature in the first half of the record and

too strong short-term responses to volcanic eruptions. The scale-free model gives a remarkably good reproduction of the large scale structure of the Moberg record and reasonable short-term volcano responses. The wavelet variance of the residuals for the two models are plotted in Fig. 7b, and again we observe that the results are consistent with a scale-free response over the millennium-long record and inconsistent with the exponential-response model.

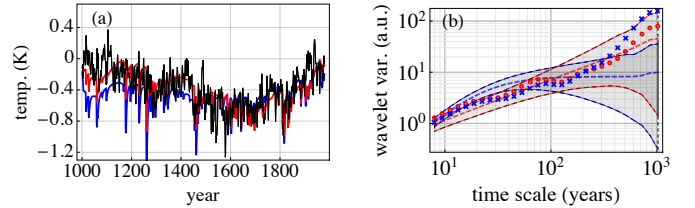


FIG. 7. (a) Deterministic part of the solution with Crowley forcing. Blue: for the exponential response model. Red: for the scale-free response model. Black: the Moberg annual temperature reconstruction record. (b) Blue crosses: Wavelet variance of Moberg record with deterministic solution of exponential response model subtracted. Red circles: the same with deterministic solution of scale-free model subtracted. Blue dashed: Ensemble mean of wavelet variance of simulated AR(1) process with estimated parameters from the exponential response model. Shaded blue area marks  $2\times$  standard deviation of the distribution of wavelet variances over the ensemble. Red dashed and shaded area: the same for an fGn process with estimated parameters from the scale-free model.

Fig. 8 shows the scale-free response to the total Crowley forcing, along with the responses to the volcanic, solar, and anthropogenic component. The most remarkable feature is that most of the cooling from the MWP to the LIA appears to be caused by volcanic cooling and not by the negative solar forcing associated with the Maunder minimum. On the other hand, the solar contribution to the warming from the LIA until mid 20'th century is comparable to the anthropogenic. After this time the warming is completely dominated by anthropogenic forcing, in agreement with what was shown in Fig. 5.

## 6. Perspectives on climate sensitivity

For predictions of future climate change on century time scales the equilibrium climate sensitivity may not be the most interesting concept. The frequency-dependent climate sensitivity  $S(f)$  given by Eq. (12) is more relevant. The transient climate response (TCR), defined as the temperature increase  $\Delta T_{tr}$  at the time of doubling of  $CO_2$  concentration in a scenario where  $CO_2$  concentration increases by 1% per year from preindustrial levels, can also readily

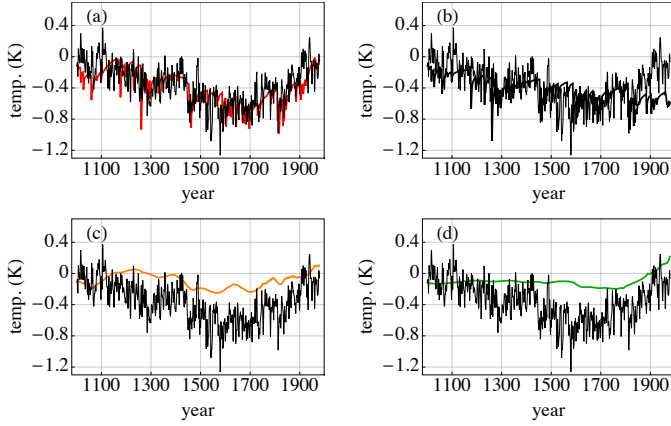


FIG. 8. Deterministic part of forced temperature change 1000-1978 A.D. according to the scale-free model with  $F(0)$  estimated from the Moberg record and  $\beta, \mu, \sigma$  from the instrumental record. Black curve is the Moberg record. (a) From total forcing. (b) From volcanic forcing. (c) From solar forcing. (d) From anthropogenic forcing.

be computed from the response models. In Fig. 9a this forcing is shown as the dotted curve to the left (the forcing is logarithmic in the  $\text{CO}_2$  concentration, so the curve is linear). The response curves to this forcing according to the two response models are shown as the blue and red dotted curves to the left in panel (b). The end of these curves (at the time of  $\text{CO}_2$  doubling after 70 yr) the temperatures represent the respective TCRs. They are both in the lower end of the range presented by the IPCC (2007). A more useful definition is to consider the response to the same  $\text{CO}_2$  increase from the present climate state that is established from the historical forcing since preindustrial times. This response is what is shown as the blue and red full curves in Fig. 9b for the next 70 yr. For the scale-free model the temperature in year 2010 lags behind the forcing due to the memory effects, and the energy flux imbalance  $dQ/dt$  established by the historical evolution at this time gives rise to a faster growth in the temperature during the next 70 yr, compared to the  $\text{CO}_2$  doubling scenario starting in year 1880.  $\Delta T_{\text{tr}}$  (according to the modified definition) is 1.3 K in the exponential response model, but 2.1 for the scale-free model. The latter is very close to the median for the TCR given in IPCC (2007). Another illustration of the memory effect can be seen from the forcing scenario where the forcing is kept constant after 2010 as shown by the dashed line in Fig. 9a. The corresponding responses are given by the blue and red dashed curves in panel (b). The short time constant in the exponential model makes the temperature stabilize in equilibrium after a few years, while in the scale-free model the temperature keeps rising as  $[2\mu^{1-\beta/2} F(2010)/\beta](t-2010)^{\beta/2}$  for  $t > 2010$  yr.

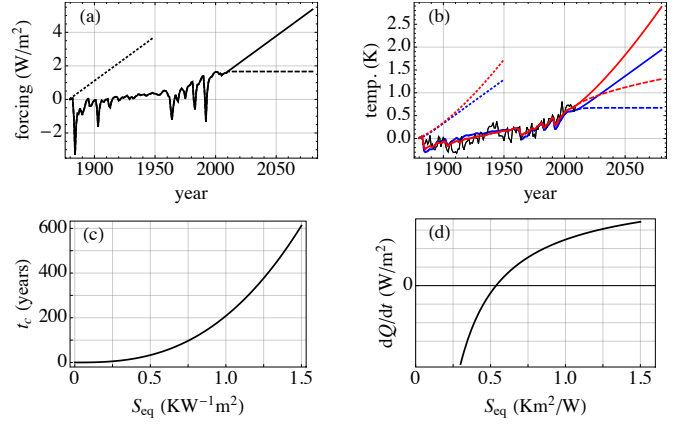


FIG. 9. (a): Dotted line is the forcing scenario corresponding to 1% increase in  $\text{CO}_2$  concentration per year starting in 1880. Solid curve is the historical forcing 1880-2010 followed by 1 % per year increase in  $\text{CO}_2$  concentration after 2010. Dashed line is forcing after 2010 kept constant at the 2010-level. (b): GMST evolution according to the two response models with parameters given in Table 1 for the three forcing scenarios described in (a). Blue curves: exponential response model. Red curves: scale-free response model. (c): The cut-off time  $t_c$  versus  $S_{\text{eq}}$  as given by equation (6) for parameters given in Table 1. (d):  $dQ/dt = F - T/S_{\text{eq}}$  at the time of  $\text{CO}_2$  doubling (year 2080) in the solid-line forcing scenario.

As discussed in section 1 this solution and Eq. (1) lead to the rather paradoxical situation of a negative energy influx  $F - T/S_{\text{eq}}$  resulting from a growing surface temperature for  $t - 2010 > t_c$ . We have plotted  $t_c$  versus  $S_{\text{eq}}$  as determined by Eq. (6) for the estimated values of  $\mu$  and  $\beta$  in Fig. 9c. For the median IPCC value  $S_{\text{eq}} = 0.75$  we have that  $t_c \approx 100$  yr, which makes the scale-free model be consistent with a positive energy influx  $dQ/dt$  throughout the entire 21st century, even if we assume the validity of Eq. (1). This is also shown in panel (d), where we have plotted the function  $F(2080) - T(2080)/S_{\text{eq}}$ , i.e., the energy influx versus  $S_{\text{eq}}$  at the time of  $\text{CO}_2$  doubling. From this plot it we observe that the energy influx is positive at this time provided  $S_{\text{eq}} > 0.5 \text{ Km}^2/\text{W}$ .

The results shown in Fig. 7b, however, suggests that scale-free response is valid at least up to millennium time scale, for which Eq. (1) and the usual estimates of the magnitude of  $S_{\text{eq}}$  would imply simultaneously negative  $dQ/dt$  and continuing rising temperatures after more than a century. Thus, on one hand we have an empirical model which consistently describes the instrumental records as well as the reconstruction records for the last millennium, and gives predictions for the 21st century in agreement with current climate models. On the other hand, predictions

made from the model for some imagined future forcing scenarios are inconsistent with conventional notions of the nature and magnitude of equilibrium climate sensitivity. A possible source of this inconsistency can be illustrated by a simple and well-known generalization of the one-box energy-balance model to a two-box model:

$$\begin{aligned} C_1 \frac{dT_1}{dt} &= -\frac{1}{S_{\text{eq}}} T_1 - \kappa(T_1 - T_2) + F \\ C_2 \frac{dT_2}{dt} &= \kappa(T_1 - T_2), \end{aligned} \quad (13)$$

where  $T_1$  could be interpreted as the temperature of the ocean mixed layer,  $T_2$  as the temperature of the deep ocean, and  $C_1$  and  $C_2$  as their respective heat capacities. For  $C_2 \gg C_1$  the response of  $T_1$  to a unit step in the forcing is

$$R_1(t) \approx S_{\text{tr}}(1 - e^{-t/\tau_{\text{tr}}}) + (S_{\text{eq}} - S_{\text{tr}})(1 - e^{-t/\tau_{\text{eq}}}), \quad (14)$$

where  $S_{\text{tr}}$ ,  $\tau_{\text{tr}}$  and  $\tau_{\text{eq}}$  are given in terms of the parameters of Eq. (13) (Rypdal 2012). Two examples of this solution are shown in Fig. 10 for different values of the longer time constant. The solution corresponding to a larger separation between the time constants of the mixed layer and the deep ocean could easily be interpreted incorrectly if integrated only up to  $t \sim \tau_{\text{tr}}$ , since the apparent time constant would be  $\tau_{\text{tr}}$  and the sensitivity  $S_{\text{tr}}$ , while the true time constant of the climate system as a whole would be  $\tau_{\text{eq}}$  and the true sensitivity would be  $S_{\text{eq}}$ . This idealized example is of course only an illustration of the principle that slowly responding components of the climate system and slow feedbacks may obscure the notion of equilibrium climate sensitivity. The true equilibrium sensitivity (if it exists) may be much larger than estimated from model runs, and hence future warming following a limited period of persistent forcing may be greater and last longer than predicted from models that do not fully take into account the LRM-properties arising from slow responses.

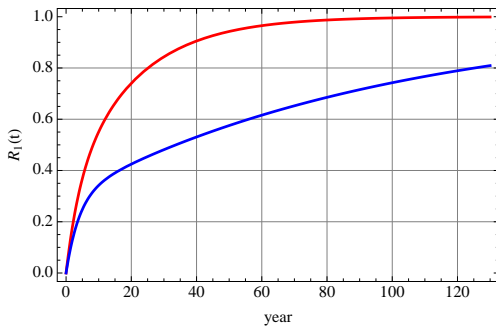


FIG. 10. The red curve is the response function  $R_1(t)$  for the two-box model with  $\tau_{\text{tr}} = 4$  years,  $\tau_{\text{eq}} = 20$  years,  $S_{\text{tr}} = 0.3 \text{ K/Wm}^{-2}$ , and  $S_{\text{eq}} = 1.0 \text{ K/Wm}^{-2}$ . The blue curve for the same parameters but  $\tau_{\text{eq}} = 100$  years.

In a recent paper Aldrin et al. (2012) supplemented the information in the time series of total forcing and temperatures of the Northern and Southern hemisphere with a series for the evolution of total ocean heat content (OHC) through the last six decades. Their response model is a simple deterministic energy-balance climate/upwelling diffusion ocean model augmented by a first-order autoregressive stochastic process for the residual. The equilibrium climate sensitivity is a parameter in the deterministic model, and since the stochastic term for the residue is AR(1) the full model cannot reproduce the LRM properties of the observed climate signal. The purpose of the work is to produce more accurate estimates of  $S_{\text{eq}}$ , and the introduction of the OHC-data is a new observational constraint on this estimate. We find it interesting to consider these data in the light of a slightly rewritten version of Eq. (1);

$$S(t) = \frac{T(t)}{\tilde{F}(t) + F(0) - dQ/dt}, \quad (15)$$

where  $S(t)$  can be thought of as a time-dependent climate sensitivity. From the observation data used in Aldrin et al. (2012) we could make crude linear trend approximations of OHC, total forcing, and global temperature, i.e.,  $dQ/dt \approx 0.25 \text{ W/m}^2$ ,  $\tilde{F}(t) \approx 0.03t \text{ W/m}^2$ , and  $T(t) \approx 0.015t \text{ W/m}^2$ , where  $t$  is time after year 1950 in units of years. Hence we have approximately,

$$S(t) \approx \frac{1}{2.0 + 66.7[F(0) - 0.25]/t}. \quad (16)$$

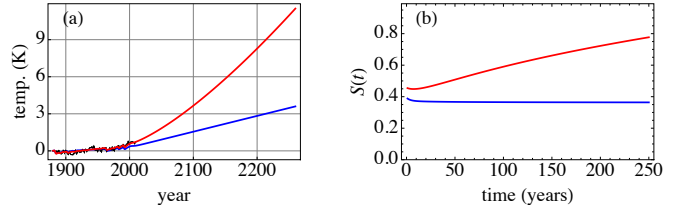


FIG. 11. (a): Global temperature evolution in response to the 1% per yr  $\text{CO}_2$  increase forcing scenario, starting in year 2010. Blue curve: the exponential response model. Red curve: the scale-free model. (b): Evolution of the time-dependent climate sensitivity  $S(t)$  in response to this forcing scenario assuming a linear increase in OHC corresponding to a net positive energy flux of  $0.25 \text{ W/m}^2$ . The time origin  $t = 0$  is year 2010. Blue curve: the exponential response model. Red curve: the scale-free model.

In Eq. (16) the initial forcing  $F(0)$  represents the deviation from radiative equilibrium in 1950, and in order to avoid vanishing sensitivity at  $t = 0$  we should have  $dQ/dt \approx F(0)$  and  $S(t) = S_{\text{eq}} \approx 0.5 \text{ Km}^2/\text{W}$ . Hence these

crude trend estimates over the last six decades yield results consistent with the existence of an equilibrium climate sensitivity very close to the best estimate of Aldrin et al. (2012). If we suppose, on the other hand, that the linear trend approximation in temperature is not quite correct, the picture may be different. Consider a linearly increasing forcing as in the future 1% CO<sub>2</sub> increase scenario shown by the full curve in Figure 9a and the same linear growth  $dQ/dt \approx 0.25$  in OHC, but assume that the temperature evolves according to the scale-free response to this forcing shown by the red full curve in Fig. 9b and in Fig. 11a. By inserting these data into Eq. (15) we obtain the time-varying climate sensitivity shown in Fig. 11b (here the time origin is chosen in year 2010). Using the temperature evolution for the exponential response shown by the blue curves in Figs. 9b and 11a yields the nearly constant climate sensitivity given by the blue curve in Fig. 11b. This demonstrates that the temperature may increase according to the power-law  $\sim t^{\beta/2+1}$  under a linearly increasing forcing and a linearly increasing OHC, provided stronger positive feedback mechanisms take effect on longer time scales and raise the climate sensitivity. In fact, this idea is just a time-domain statement of the concept of a frequency-dependent sensitivity which was formulated in section 3. The scenario of 1% increase in CO<sub>2</sub> concentration per year continued 250 years into the future is a very extreme one, and corresponds to a raise in concentration of more than one order of magnitude. Yet, our results show that within the framework of the scale-free model the global temperature may increase by more than 10 K while the OHC maintains a positive linear growth rate throughout this period with only a moderate increase in  $S(t)$  from 0.5 to 0.8. The important message from these considerations is that a time- (or frequency-) dependent climate sensitivity may raise the cut-off scale  $t_c$  in the scale-free response beyond the millennium time scale, and hence resolves the paradox that the observation data supports the existence of LRM response at least up to such scales.

## 7. Discussion and conclusions

We have in this paper considered linear models of global temperature response and maximum-likelihood estimation of model parameters. The parameter estimation is based on observed climate and forcing records and an assumption of additional stochastic forcing. This modeling shows that a scale-free response is consistent with the stochastic properties of the noisy components of the data, whereas an exponential model is not. The scale-free model with parameters estimated from the modern instrumental temperature and forcing record successfully predicts the large-scale evolution of the Moberg reconstructed temperature record when the Crowley forcing for the last millennium is used as input. Solutions for the volcanic, solar, and an-

thropogenic components of the Crowley forcing show that the model ascribes most of the temperature decrease from the MWP to the LIA to the volcanic component, while the rise from the LIA to year 1979 is attributed to both solar and anthropogenic forcing up till about year 1950 and to anthropogenic after this time. The prediction is not completely independent of the Moberg and Crowley records, however, since the forcing  $F(0)$  indicating the departure from climate equilibrium at year 1000, must be estimated from these data.

Planet Earth is a non-equilibrium driven physical system which radiates energy freely to space. Even when the drive (forcing) is constant in time the total energy content of the system will fluctuate, and if these fluctuations are large on time scales beyond a century it may have little meaning to operate with the notion of an equilibrium climate sensitivity. Thus, the long-range dependence in the climate response implies that the equilibrium climate sensitivity concept needs to be generalized to encompass a time-scale dependent sensitivity which incorporates the effect of increasingly delayed positive feedbacks. This may have far-reaching implications for our assessment of future global warming under strong anthropogenic forcing sustained over centuries, as illustrated by the difference between the projected warming according to the scale-free and exponential response models shown in Fig. 11a.

The importance of the “background” continuum of time scales in climate variability has been stressed by Lovejoy and Schertzer (2013). In a short review of their own work Lovejoy (2013) shows results based on application of their Haar structure function technique to instrumental and multiproxy temperature records. For instrumental records they find a spectral plateau of  $\beta \approx 0.8$  on time scales up to a decade, but the a sharp transition to  $\beta \approx 1.8$  on longer time scales. For the multiproxy records they find a similar transition after a few decades. By similar analysis of ice-core data they also obtain  $\beta \approx 1.8$  on time scales greater than a millennium, and argue that this transition constitutes the separation between a macroweather regime to a climate regime. The analysis presented here does not support that such a transition in the scaling properties of internal variability takes place on decadal time scales in global or hemispheric records. These scaling properties are shown by the wavelet variances of the residuals in Figs. 3b and 7b, and indicate  $\beta \approx 0.8$ -scaling through the entire instrumental century-long record and the millennium-long multiproxy record, respectively. The transition on multi-decadal time scale also fails to show up in the detrending scaling analysis of proxy data in Rybski et al. (2006) and Rypdal et al. (2013). We suggest that the transition reported by Lovejoy (2013) is a consequence of not distinguishing between forced and stochastic response (alternatively, by not properly eliminating “trends” imposed by external forcing). A transition to a more persistent cli-

mate regime may perhaps be identified on millenium time scales, but it is an open and interesting question whether the rise of  $\beta$  from a stationary ( $\beta < 1$ ) to a non-stationary regime ( $\beta > 1$ ) is an actual change in the properties of the climate response or an effect of trends imposed by orbital forcing.

It is important to keep in mind that what we do in this paper is only to select the optimal model from two classes of linear response models when the selection criterion is the model's tendency to reproduce the observed climate record from a given forcing record. It is possible that other classes would contain models that perform better, and the results are of course not better than the data. The nature of the matter is that the results can be improved from better models, and better and more data, and our understanding is of course incomplete until the delayed feedbacks responsible for the long-range dependence are identified and described from physical principles.

## APPENDIX

### Maximum-likelihood estimation

In discretized versions the dynamic-stochastic models defined by equation (3) can be written on the form

$$\mathbf{T} = G\mathbf{F} + \mathbf{x},$$

where  $\mathbf{T} = (T_1, T_2, \dots, T_n)$  is the random vector representing the temperature record and  $\mathbf{F} = (F_1, \dots, F_n)$  is the deterministic component of the forcing, i.e.  $T_i = T(i\Delta t)$  and  $F_i = F(i\Delta t)$  where  $\Delta t$  is the time-resolution of the records. The matrix  $G$  is defined from the Green's function by  $G_{ij} = G((i-j)\Delta t)$ , and the vector  $\mathbf{x} = (x_1, \dots, x_n)$  is a stochastic process. For the exponential response model  $\mathbf{x}$  is an AR(1) process

$$x_{k+1} = ax_k + \phi\varepsilon_k,$$

where  $\phi = \sigma/C$ ,  $a = 1 - 1/\tau$ , and  $\varepsilon_k$  are i.i.d. Gaussian variables of unit variance. In the scale-free model the process  $\mathbf{x}$  is an fGn. To emphasize the parameter dependence we denote the AR(1) process by  $\mathbf{x}_{C,\sigma,\tau}$  and the fGn by  $\mathbf{x}_{\mu,\sigma,\beta}$ . In the same way we denote the Green's function by  $G_{C,\tau}$  in the exponential response model, and by  $G_{\mu,\beta}$  in the scale-free response model.

By a simple change of variables the  $n$ -dimensional probability density function (pdf) of the random vector  $\mathbf{T}$  is related to the pdf of  $\mathbf{x}$  through

$$p_{\mathbf{T}}(\mathbf{T}) = p_{\mathbf{x}}(\mathbf{T} - G\mathbf{F}).$$

For temperature observations  $\mathbf{T}$  the likelihood function for the exponential response model becomes

$$L(C, \sigma, \tau) = p_{\mathbf{x}_{C,\sigma,\tau}}(\mathbf{T} - G_{C,\tau}\mathbf{F}), \quad (\text{A1})$$

and for the scale-free response model:

$$L(\mu, \sigma, \beta) = p_{\mathbf{x}_{\mu,\sigma,\beta}}(\mathbf{T} - G_{\mu,\beta}\mathbf{F}). \quad (\text{A2})$$

We see that computation of these likelihoods essentially entails computation of corresponding likelihoods for AR(1) models and fGns. Computation of likelihood functions for auto-regressive processes is straight forward using standard time-series techniques. Effective computation of the likelihood function for fGns can be achieved using the Durbin-Levinson algorithm for inverting the co-variance matrix (McLeod et al. 2007).

In this paper the parameters of the two models are estimated by maximizing Eqs. (A1) and (A2) numerically.

## REFERENCES

- Aldrin, M., M. Holden, P. Guttorp, R. B. Skeie, G. Myhre, and T. K. Berntsen, 2012: Bayesian estimation of climate sensitivity based on a simple climate model fitted to observations of hemispheric temperatures and global ocean heat content. *Environmetrics*, **23** (3), 253–271.
- Beran, J., 1994: *Statistics for long-memory processes*. Monographs on statistics and applied probability, Chapman & Hall/CRC, Boca Raton.
- Brohan, P., J. J. Kennedy, I. Harris, S. F. B. Tett, and P. D. Jones, 2006: Uncertainty estimates in regional and global observed temperature changes: A new data set from 1850. *J. Geophys. Res.*, **111** (D12), D12106.
- Crowley, T. J., 2000: Causes of Climate Change Over the Past 1000 Years. *Science*, **289** (5477), 270–277.
- Embrechts, P. and M. Maejima, 2002: *Selfsimilar Processes*. Princeton University Press, Princeton.
- Flandrin, P., 1992: Wavelet analysis and synthesis of fractional Brownian motion. *IEEE Trans. Inform. Theory*, **48**, 910–917.
- Hansen, J., M. Sato, P. Kharecha, and K. von Scuckmann, 2011: Earth's energy imbalance and implications. *Atmospheric Chemistry and Physics*, **11**, 13 421–13 449.
- Hansen, J., et al., 2005: Efficacy of climate forcings. *J. Geophys. Res.*, **110** (D18), D18104.
- Held, I. M., M. Winton, K. Takahashi, T. Delworth, F. Zeng, and G. K. Vallis, 2010: Probing the Fast and Slow Components of Global Warming by Returning Abruptly to Preindustrial Forcing. *J. Climate*, **23** (9), 2418–2427.
- IPCC, 2007: Climate Change 2007: The Physical Science Basis. Tech. rep., Geneva.

- Lovejoy, S., 2013: What Is Climate? *Eos Trans. AGU*, **94** (1), 1–2.
- Lovejoy, S. and D. Schertzer, 2013: *The Weather and Climate: Emergent Laws and Multifractal Cascades*. Cambridge University Press.
- McLeod, I. A., H. Yu, and Z. L. Krougly, 2007: Algorithms for Linear Time Series Analysis: With R Package . *J. Stat. Softw.*, **23** (5).
- Moberg, A., D. M. Sonechkin, K. Holmgren, N. M. Datsenko, and W. Karlen, 2005: Highly variable Northern Hemisphere temperatures reconstructed from low- and high-resolution proxy data. *Nature*, **433**, 613–617.
- Rybski, D., A. Bunde, S. Havlin, and H. von Storch, 2006: Long-term persistence in climate and the detection problem. *Geophys. Res. Lett.*, **33** (6), L06718.
- Rypdal, K., 2012: Global temperature response to radiative forcing: Solar cycle versus volcanic eruptions. *J. Geophys. Res.*, **117** (D6), D06115.
- Rypdal, K., L. Østvand, and M. Rypdal, 2013: Long-range memory in Earth’s surface temperature on time scales from months to centuries. *J. Geophys. Res. Atmos.*, in press.